Amino Acids (2012) 42:2019–2030
DOI 10.1007/s00726-011-0933-z

ORIGINAL ARTICLE

Electrostatics of folded and unfolded bovine β-lactoglobulin

Ivano Eberini · Cristina Sensi · Alberto Barbiroli · Franco Bonomi · Stefania Iametti · Monica Galliano · Elisabetta Gianazza

Received: 31 March 2011 / Accepted: 30 April 2011 / Published online: 26 May 2011

Abstract We report on electrophoretic, spectroscopic, and computational studies aimed at clarifying, at atomic resolution, the electrostatics of folded and unfolded bovine β-lactoglobulin (BLG) with a detailed characterization of the specific aminoacids involved. The procedures we used involved denaturant gradient gel electrophoresis, isoelectric focusing, electrophoretic titration curves, circular dichroism and fluorescence spectra in the presence of increasing concentrations of urea (up to 8 M), electrostatics computations and low-mode molecular dynamics. Discrepancy between electrophoretic and spectroscopic evidence suggests that changes in mobility induced by urea are not just the result of changes in gyration radius upon unfolding. Electrophoretic titration curves run across a pH range of 3.5–9 in the presence of urea suggest that more than one aminoacid residue may have anomalous pK_a value in native BLG. Detailed computational studies indicate a shift in *pK*a of Glu44, Glu89, and Glu114, mainly due to changes in global and local desolvation. For His161, the formation of hydrogen bond(s) could add up to desolvation contributions. However, since His161 is at the C terminus, the end-effect associated to the solvated form strongly influences its pK_a value with extreme variation between crystal structures on one side and NMR or low-mode molecular dynamics structures on the other. The urea concentration effective in BLG unfolding depends on pH, with higher stability of the protein at lower pH.

Keywords Bovine β-lactoglobulin · Electrostatics · Unfolding · Urea · Electrophoresis · Molecular modeling

Abbreviations

BLG	Bovine β-lactoglobulin
Chg	Component of the pK_a due to buried charge–charge interactions
DGGE	Denaturant gradient gel electrophoresis
ETC	Electrophoretic titration curve
GDes	Component of the pK_a due to global desolvation of the group
HB	Component of the pK_a due to hydrogen bonds, including strong hydrogen bonds between buried groups
LDes	Component of the pK_a due to local desolvation
NGlob	Number of atoms within a 15.5 Å radius (it is a measure of bulk burial: atoms with NGlob >400 are considered to be buried)
NLoc	Number of atoms within a local radius, varying from 3.5–6.0 Å (it is used to estimate the solvent accessible surface of the group)
*pK*a	Predicted pK_a value of the group according to the MOE Residue pK_a program
ΔpK_a	(pK_a unfolded − pK_a native)

Electronic supplementary material The online version of this article (doi:10.1007/s00726-011-0933-z) contains supplementary material, which is available to authorized users.

I. Eberini · C. Sensi · E. Gianazza (✉)
Gruppo di Studio per la Proteomica e la Struttura delle Proteine, Dipartimento di Scienze Farmacologiche, Università degli Studi di Milano, via Giuseppe Balzaretti 9, 20133 Milan, Italy
e-mail: elisabetta.gianazza@unimi.it

A. Barbiroli · F. Bonomi · S. Iametti
Sezione di Biochimica, Dipartimento di Scienze Molecolari Agroalimentari, Università degli Studi di Milano, via Celoria 2, 20133 Milan, Italy

M. Galliano
Dipartimento di Biochimica "Alessandro Castellani", Università degli Studi, via Taramelli 3B, 27100 Pavia, Italy

pK model	Intrinsic pK_a of the group (the component which is independent of environment)
TC	Titration curve

Introduction

The provocative title of a 2006 paper asks: Why are proteins charged? (Gitlin et al. 2006). Several reports answer the question: overall surface charge as well as ionization of individual residues are key determinants of protein localization, association, and function (Goldenberg and Steinberg 2010).

Electrostatic interactions affect subcellular targeting and contribute to the organization of integral and peripheral membrane proteins in, or next to, lipid bilayers (Mulgrew-Nesbitt et al. 2006). Electrostatic interactions govern thermodynamic and kinetic aspects of the formation of protein:protein supramolecular assemblies (Schreiber et al. 2006). Electrostatic interactions play a role in folding, solubility and thermal stability, conformational adaptability and movement of individual proteins, and in enzyme activity and binding energies (Aguilar et al. 2010; Harris and Turner 2002; Pace et al. 2009). In brief, electrostatic interactions are at the core of all types of molecular recognition (Nakamura 1996). Protein electrostatics has been experimentally addressed (Lee and Crippen 2009; Nielsen and McCammon 2003; Pace et al. 2009; Tanford 1962) and more and more often modeled in silico (Juffer 1998; Neves-Petersen and Petersen 2003; Vizcarra and Mayo 2005).

An aspect insufficiently covered by current scientific literature is the electrostatics of misfolded/unfolded proteins. Simulating, at atomic level, the loss of structure brought about by the presence of a chaotropic agent is computationally intensive when the molecule has in fact the size of a protein, however small (instead of a peptide). Some of the experimental approaches actually probe the sample in bulk and provide information on average rather than individual behavior of the dissociating groups.

Partial unfolding, often resulting in protein aggregation, is relevant to several processes. In vivo, among the general strategies for controlling such problem (Tyedmers et al.), intracellular (Ellis and van der Vies 1991) and extracellular (Wilson et al. 2008) chaperones specifically bind, whereas proteasomes (Goldberg 2003) specifically degrade stressed proteins. A peculiar example is connected with Alzheimer's disease (AD): fibroblasts derived from AD patients express an altered conformational status of p53, and the exposure to nanomolar concentrations of amyloid β 1–40 induces the expression of an unfolded p53 protein isoform in fibroblasts derived from non-AD subjects (Lanni et al. 2007). Even more common, the occurrence of misfolded proteins during industrial processes [as exemplified by protein aggregation by heat and other physical treatments (Iametti et al. 1996; Iametti et al. 2002)] and in the field of protein-based nanotechnology [as exemplified by the assembly of fibrils, tubules, and other nanostructures from partially denatured bovine β-lactoglobulin (BLG) (Rasmussen et al. 2007)].

Sometime ago, some of us published a comprehensive assessment of the pH-dependence of several structural and functional features of BLG (Beringhelli et al. 2002). As part of Supporting information (Figure S2), we posted the patterns of the protein in denaturant gradient gel electrophoresis (DGGE), i.e., after migration across a transverse urea gradient in buffers at different pH (Creighton 1979). The picture included the images from runs at pH 4.8 and 6.1, and the contrast between the two patterns has since suggested an in-depth investigation on the reason(s) underlying such a sharp change across just more than 1 pH unit. We carried out this investigation through a combination of electrophoretic and spectroscopic techniques, and here we are interpreting the results in the light of the detailed physicochemical data we could evaluate for electrostatics of folded and unfolded BLG with computational procedures. The interpretation of DGGE experiments carried out with neutral chaotropic agents like urea is usually focused on the effects on the gyration radius of the proteins. For BLG in the tested pH range, the variation of the hydrodynamic volume is only one of the components to the differential mobility of the unfolded protein, and the pK_a shifts between folded and unfolded state for some of the BLG residues also play a relevant role in the observed protein behavior.

Materials and methods

BLG purification

Isoforms A and B of BLG were purified from cow milk according to (Monaco et al. 1987) and defatted by treatment on a Lipidex-1000 (Perkin-Elmer) column. Both were subjected to DGGE experiments and used for pK_a computations; isoform B was more thoroughly investigated in its unfolding behavior.

Zonal electrophoresis across a transverse urea gradient

BLG denaturation curves were evaluated by running the purified protein, 0.5 mg/mL in 10 mMol/L phosphate/Na pH 7.4, across 0–8 M urea gradients (Creighton 1979). The gels were cast on GelBond PAG foils, in a 0.5-mm thick cassette. Sample application trenches, 90 × 3 mm, were shaped in a mold with strips of embossing tape. A denaturant gradient, 65 mm high and corresponding to

4.5 + 4.5 mL solution, was cast between two 2 cm high concentration plateaus.

In all gels, the polyacrylamide matrix had a concentration of T5 C4. pH and buffer composition (Goldenberg 1989), as well as running conditions, varied from one experiment to another (migration lasting in all cases for 120 min) to take into account the kinetic parameters of the folding–unfolding transition (Creighton 1980). For the two extremes: (1) buffer pH 4.8 = 80 mM γ-aminobutyric acid/20 mM acetic acid (conductivity = 1.705 mS/cm); run for 1,000 Vh; (2) buffer pH 6.1 = 30 mM histidine/30 mM 2-[*N*-morpholino] ethanesulfonic acid, MES (conductivity = 2.055 ms/cm); run for 600 Vh. Intermediate values, 0.1 pH unit apart, were obtained by proportional mixing of the two buffers above, and running conditions were linearly interpolated (step = 40 Vh). Gels were subjected to electrophoresis at 288 K, in a horizontal chamber (Multiphor II, Pharmacia), with an electrode distance of 19.5 cm and agarose strips as anolyte and catholyte. Protein staining was done with 0.3% w/v Coomassie Blue R250 in 30:10:60 v:v:v ethanol:acetic acid:water.

Isoelectric focusing

An immobilized pH gradient (IPG) (Bjellqvist et al. 1982) covering the range of 4–10 with a non-linear course (Gianazza et al. 1985) was polymerized and then washed and dried according to standard protocols (Righetti 1990). Strips of the gel were then re-swollen in urea solutions of increasing concentration. The gel was run at 15°C for 15,000 Vh. Coomassie staining was carried out according to Righetti and Drysdale (1974).

pH mobility curves

The pH mobility (or electrophoretic titration) curves (ETC) (Gianazza et al. 1999; Righetti and Gianazza 1980; Rosengren et al. 1977) of BLG isoform B under varying conditions were evaluated by running the protein across a wide pH range set by focused carrier ampholytes. Empty gels, with a T5 C4 matrix, were cast in a mold similar to that described above (DGGE section), washed, dried and then re-swollen in solutions containing 2% w/v ampholine 3.5–10 and appropriate concentrations of urea. The first dimension run lasted 1 h at 15°C, and the pH gradient was established in the gel by delivering a constant power of 5 W over an anode–cathode distance of 10 cm. BLG was loaded after dilution to 1.2 mg/mL in either buffer or 8 M urea. The run, orthogonal to the direction of the pH gradient, was at 690 V over an anode–cathode distance of 23 cm, with a duration increasing from 20 min in the absence of additives to 60 min in the presence of 8 M urea. After extensive washing with in 30:10:60 v:v:v of ethanol:acetic acid:water to remove most carrier ampholytes, the protein pattern was stained with Coomassie Blue R250 according to Righetti and Drysdale (1974).

Circular dichroism and fluorescence spectra

Near UV CD spectra of BLG isoform B were recorded in 1-cm pathlength cells at protein concentrations in the 1 mg/mL range on a Jasco J810 spectropolarimeter equipped with computer-controlled, Peltier-driven cell holders, and analyzed by means of the Jasco J800 software. Individual dilutions of the protein into various buffer solutions containing the appropriate urea concentration were used.

Tryptophan fluorescence emission spectra were collected with an excitation at 298 nm in a Perkin-Elmer LS50 spectrofluorometer, also equipped with computer-controlled, Peltier-driven cell holder, on protein solutions in the 0.1 mg/mL range.

Prediction of aminoacid pK_a

pK_a values for all the titratable residues were computed through the Residue pK_a program of the Biopolymer module in the Molecular Operating Environment (MOE), version 2009.10. This program was based on the PROPKA method (Li et al. 2005), which evaluates the empirical shifts in pK_a values associated with the different types of interactions that each group may establish. Values can be computed very rapidly as a simple pairwise scoring function.

$$pK_a = pK_{aq} + \Delta pK_{des} + \Delta pK_{HB} + \Delta pK_{chgchg}$$

where pK_{aq} is the pK_a value of the free residue in aqueous solution, ΔpK_{des} is the desolvation component (both global and local desolvations are measured as a function of burial), ΔpK_{HB} is the hydrogen bonding contribution, and ΔpK_{chgchg} is the buried charge–charge interaction component.

The pK_a prediction algorithm is iterative. An initial set of pK_a values is computed, and then the charge–charge interactions and the hydrogen bond terms between groups with similar pK_a values are recomputed. As a rule, the group with the higher pK_a will lower that of the interacting partner, while its own pK_a will increase by a corresponding amount. Once this is done for all relevant pairwise interactions, the process is repeated until it converges.

The program was run on four structures: the native BLG isoform A as crystallized at acidic pH (RCSB PDB ID: 3BLG), and its unfolded form; the native BLG isoform B as crystallized at neutral pH (RCSB PDB ID: 1BSQ), and its unfolded form. The protonation states of the various protein forms were computed at pH 5, which is the pH value closest to the theoretical p*I* (see "Results"). The

aforementioned unfolded forms were produced by simulating the protein molecular dynamics (MD) at a very high temperature (1,000 K for 150 ps, in a NVT ensemble, with the CHARMM27 force field and an implicit Generalized Born solvation model). Furthermore, all the remaining BLG structures available from the RCSB database (http://www.rcsb.org/pdb/home/home.do) were submitted to the same computational procedure for obtaining the value of His161 pK_a in the various native forms.

Low-mode molecular dynamics

For studying the flexibility of the BLG C terminus, we applied the low-mode molecular dynamics (LowModeMD) approach, aimed at focusing a MD trajectory along the low-mode vibrations and featuring a very efficient way versus classical MD for searching for minima troughs on the potential energy surface. To run these computations, we used the MOE Conformational Search program of the Conformations module. This program uses an efficient implicit method for estimating the low-frequency modes and is based on the attenuation of high-range velocities as described in detail in (Labute 2010).

The six C-terminal residues of 3BLG were left free to move during the LowModeMD, whereas the residues more than 4.5 Å away were fixed (not free to move, but used for the energy calculations); the other residues were defined as inert (fixed and not used for energy calculations). The simulation was carried out with default parameters, except for strain cutoff, which was set at 60 kcal/mol. One hundred conformations of the C terminus were generated and ranked according to the value of the potential energy of the conformation. Only 11 conformations with the same stereochemistry configuration and with strain energy relative to the lowest energy conformation lower than 2 kcal/mol were analyzed. For all these conformations, the pK_a values for His161 were calculated as described earlier.

Results

Creighton's group has not only laid the theoretical basis for DGGE (Creighton 1979, 1980), but also defined the optimal experimental conditions for the runs, including the selection of a few low conductivity, high buffering capacity media of different pH [3.8, 4.8, 6.1, 7.4, 8.7 (Goldenberg 1989)], which are since in common use, including by our lab (Beringhelli et al. 2002; Gianazza et al. 1997). Running DGGE on BLG isoform B at pH 6.1 across a 0–8 M urea gradient results in the denaturation curve shown in the rightmost panel in the lower row of Fig. 1. Such a sigmoidal pattern (specifically, region *g* of the curve) implies a cooperative transition between the native and unfolded states, whereas the continuous trace entails an essentially reversible course of the transition and sets an upper limit to its duration at 12 min (i.e., at 1/10 of the duration of the run). A small amount of unfolded BLG (migrating in region *i*) is kinetically trapped in the unfolded state.

Essentially, none of these features is present in the denaturation curve of BLG when DGGE is run at a pH of 4.8, as shown in the leftmost panel of the upper row in Fig. 1. This suggests that the folding–unfolding transition may have peculiar features at acidic pH. However, DGGE migration even at lower pH, 3.8, produces a sigmoidal

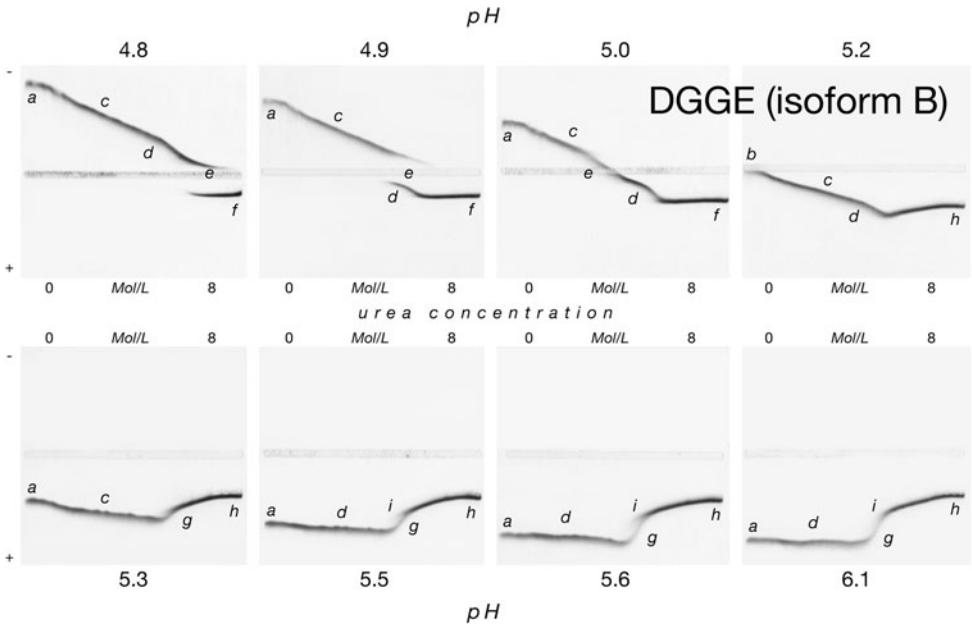

Fig. 1 DGGE of BLG B across 0–8 M transverse urea gradient at increasing pH (see *top* and *bottom rows*). Application trenches in the middle; polarity as marked (*left*)

curve (Beringhelli et al. 2002). Similar contrasting findings are observed also for BLG isoform A (Fig. 2).

To investigate this seemingly inconsistent behavior, we monitored the unfolding of BLG isoform B through the analysis of its CD and fluorescence spectra in the presence of increasing concentrations of urea in the range 0–8 M and at the same pH values as in DGGE. On contrary to electrophoresis, spectroscopic data (Fig. 3) may be plotted in all cases along a sigmoid curve, pointing to a simple cooperative transition at both pH 4.8 and 6.1. At pH 4.8, BLG unfolding was carried out in the two different buffer media, namely acetic acid/GABA—used in electrophoretic runs—and acetic acid/Na, with identical results.

The discrepancy between electrophoretic and spectroscopic evidence suggests that the interpretation of changes in mobility in DGGE as resulting only from changes in gyration radius upon unfolding is inadequate. Most likely, in this case, DGGE monitors the compound effect of two or more phenomena affecting the protein mobility. To investigate this point in better detail, we monitored the behavior of BLG in DGGE across the pH range 4.8–6.1 in 12 more experiments, run in buffers at 0.1 pH unit apart. Six representative patterns are collected in Fig. 1 for isoform B and in Fig. 2 for isoform A. Gradual changes are observed for a number of features with increasing pH, until around pH 5.5 the pattern becomes indistinguishable from that at pH 6.1.

In detail, for BLG isoform B in the plateau without urea, migration is towards the cathode at lower pH, towards the anode at higher pH (refer to region *a* of the curves). In the plateau at 8 M urea, migration is towards the anode in all runs (region *h*). Thus, over the analyzed pH range, the native protein titrates from cation to anion, whereas the denatured protein is an anion all throughout. The isoionic point of the native protein was evaluated at pH 5.2, as at this pH it does not migrate from the application trench (detail *b*); the isoionic point of the denatured protein is <4.8 [and >3.8 (Beringhelli et al. 2002)].

The denaturation pattern observed between pH 4.8 and 5.2–5.3 includes several peculiar features. A short portion of the curve (region *d*) approaches a sigmoidal course; the position of its midpoint shifts from 6 M urea at pH 4.8 to 5 M urea at pH 5.2. At pH 4.8, region *d* sees a decrease of BLG mobility as a cation, whereas at pH 4.9–5.2 it sees an increase of mobility as an anion: this feature is opposite to the change associated with an increase in gyration radius upon unfolding. Between pH 4.8 and 5.3, region *d* is preceded by a portion of the curve (region *c*) over which the mobility of the protein changes as a linear function of urea concentration; between pH 4.8 and 5.0 it is followed by a region over which the mobility of the protein is constant (mobility plateau) (region *f*). A sharp discontinuity in the curve (detail *e*) is observed just after the sigmoidal section (*d*) at pH 4.8, just before at pH 4.9; at pH 5.0 a deformation of the curve marks the transition between region *c* and *d*.

As already commented, at pH ≥5.5, the denaturation curve has a typical sigmoidal shape (specifically refer to detail *g*) with the only peculiarity that BLG mobility further decreases at higher urea concentrations (region *h*) while it is constant at lower urea concentrations (region *d*). These details are also observed with all runs in media at pH >6.1 (Beringhelli et al. 2002). The overall trend is similar for BLG isoform A (Fig. 2); the isoionic point is in this case around pH 5.0.

The DGGE data across the sampled pH range imply a difference in p*I* between native and unfolded BLG, both for

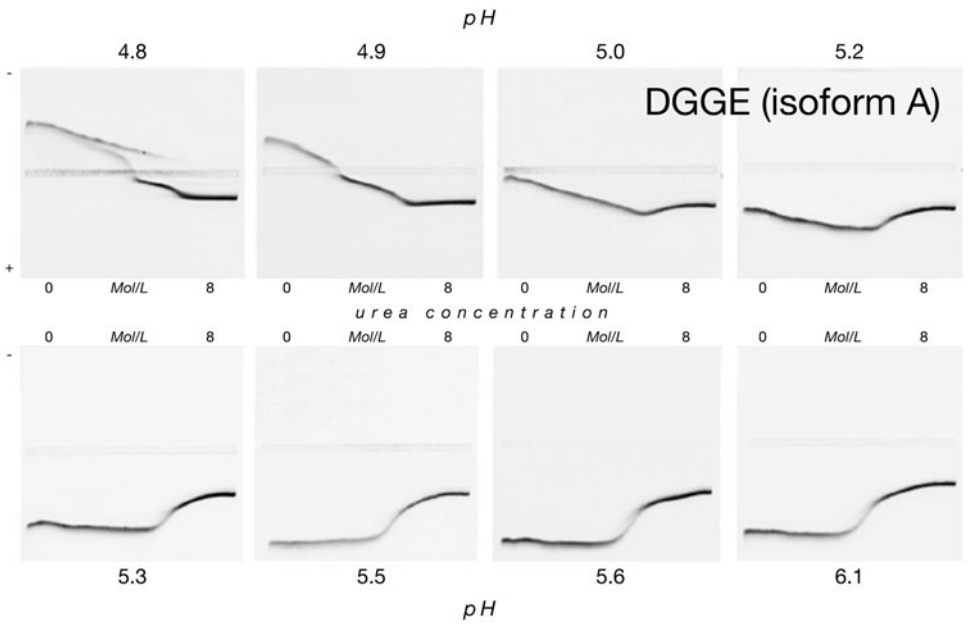

Fig. 2 DGGE of BLG A across 0–8 M transverse urea gradient at increasing pH (see *top* and *bottom rows*). Application trenches in the middle; polarity as marked (*left*)

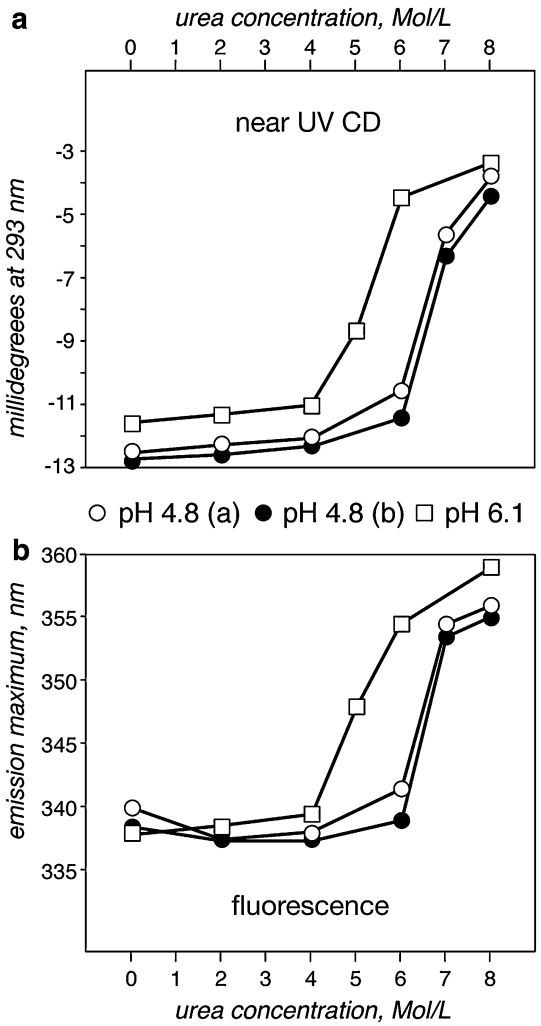

Fig. 3 **a** Circular dichroism as a function of urea concentration, at pH 4.8 (**a** in acetic acid/GABA; **b** in acetic acid/Na) and at pH 6.1. **b** Fluorescence emission as a function of urea concentration, at pH 4.8 (**a** in acetic acid/GABA; **b** in acetic acid/Na) and at pH 6.1

isoform A and isoform B. Indeed, as shown in Fig. 4a, isoelectric focusing of isoform B in the presence of either no additive or 8 M urea (leftmost and rightmost lanes) demonstrates a higher p*I* for native than for unfolded BLG. In either of these limit conditions only a single, sharp band may be stained. On the contrary, both these two bands are present, in varying ratios, together with further, minor components, at intermediate urea concentrations (central lanes). Together with the dark background staining, this evidence suggests the existence of a shifting equilibrium among non-native BLG conformers, each with a different p*I*.

To investigate the effect of solvent on aminoacid dissociable groups as the basis for this p*I* shift, we run ETC across the 3.5–9 pH range, in the presence of urea concentrations between 0 and 8 M. Figure 4b compares the five paired patterns resulting from loading BLG isoform B sample in plain buffer or in 8 M urea. Comparison between curves allows to verify whether equilibrium condition has been attained in the protein structure and, when this is not the case, to comment on the pH dependence of (re)folding occurring throughout the duration of the electrophoretic run.

The panel corresponding to 8 M urea concentration shows two parallel curves, and demonstrates that a 60 min exposure (the duration of the electrophoretic migration) is sufficient to completely unfold BLG at any pH between 3.5 and 9. The titration curve (TC) of native BLG (panel 0 M urea, sample in buffer) differs from the curve of unfolded BLG (panel 8 M urea, both samples) in its overall shape, as summarized in Supplementary Figure 1. While the latter may be approximated to two linear portions connected by an ark, the former bends in a more gradual way across the alkaline pH range. This implies that some charged aminoacids have different pK_a in either folded or unfolded BLG.

In order to verify this hypothesis, we carried out an in silico pK_a value prediction for all the titratable aminoacids of BLG isoforms A and B in their native and unfolded forms. Results of these calculations are reported in Table 1. The PROPKA method, described in the "Materials and methods", estimates the contribution of the different types of interactions on the pK_a of each individual residue. These include effects of global (GDes) and local desolvation (LDes) of the group, of bulk burial (NGlob), of solvent accessible surface (NLoc), and the contribution of hydrogen bonds (HB) and buried charge–charge interactions (Chg). These additional data are reported in Supplementary Table 1 whose legend also provides a more detailed definition of all the above parameters.

In Table 1, we have highlighted all the residues—namely, Glu44, Glu89, His161 both for A and B isoforms, and Glu114 only for A isoform—that satisfy the following relationship:

$$\left(pK_{\text{ajfolded}} < theoretical\, pI < pK_{\text{ajunfolded}}\right) \cup \left(pK_{\text{ajunfolded}} < theoretical\, pI < pK_{\text{ajfolded}}\right) \quad (1)$$

This is useful for selecting a subset of residues whose native and unfolded pK_a values define an interval, which includes the protein native p*I* value. These aminoacids are most likely to be involved in the observed p*I* shift between the native and the unfolded form of BLG.

The theoretical p*I* for native BLG isoforms were computed according to the method described in (Sillero and Maldonado 2006) with a C++ program written in our lab; they were estimated, respectively, at 4.76 for isoform A and at 4.84 for isoform B. All the above residues, except Glu114 of isoform A and Glu44 of isoform B, also satisfy the following relationship:

$$\left|\Delta pK_{\text{aj}}\right| \geq 1 \quad (2)$$

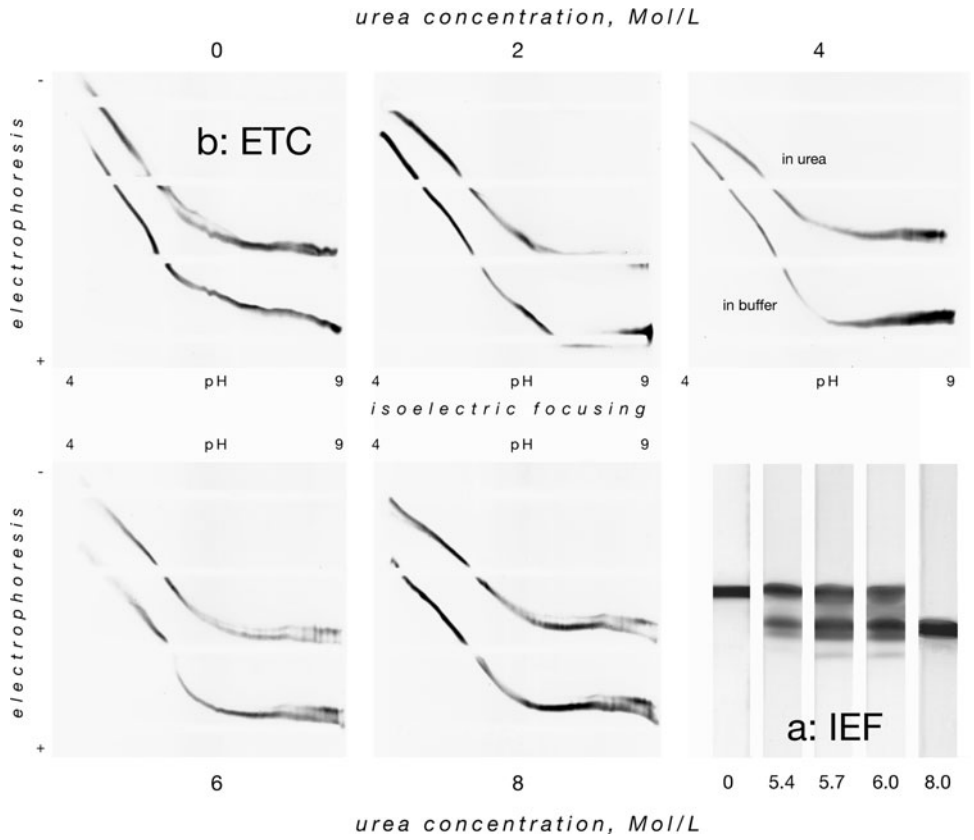

Fig. 4 **a** Isoelectric focusing of BLG isoform B in the presence of increasing urea concentrations (*bottom row*). **b** ETC of BLG isoform B across a transverse pH gradient in the presence of increasing urea concentrations (*top* and *bottom rows*). Protein dissolved in buffer was loaded in the lower sample trench, protein dissolved in 8 M urea in the upper sample trench. Polarity as marked

thus showing a significant pK_a variation between native and unfolded BLG. These large shifts in pK_a values, both for the A and B isoforms, can be ascribed to the different environment surrounding the specified residues in the native versus the unfolded form.

All the five highlighted aminoacids may be classified as buried in native BLG isoforms as they are associated with NGlob values >400. Conversely, all of them have NGlob <400, hence are solvent exposed, in the BLG unfolded isoforms (refer to the corresponding columns in Supplementary Table 1A and B). The high measured bulk burial significantly contributes to the pK_a shift due to global desolvation of the corresponding dissociable groups (GDes value in the native BLG sections of Supplementary Table 1).

For both the native A and B isoforms, His161 shows the highest NLoc values (39 and 41, respectively), suggesting that this residue has a very small solvent accessible surface. This is associated to a very high contribution of local desolvation to the pK_a value (−2.73 and −2.87, respectively) (LDes column in the native BLG sections of Supplementary Table 1). This parameter appears much less critical for the other three aminoacids.

The formation of hydrogen bonds can also contribute to the computed pK_a values: Glu89 in the native isoform A (−0.32) and His161 for both native isoforms are involved in relevant hydrogen bonds able to significantly influence their pK_a values (1.01 and 1.14 for isoform A and B, respectively; HB column in the native BLG sections of Supplementary Table 1).

All the local structural contributions detected in the BLG native isoforms are almost completely lost after the unfolding process (see Supplementary Table 1). Hence, the ΔpK_a values of the selected residues between native and unfolded BLG can explain the different p*I* observed in 0 M (native) versus 8 M urea (unfolded).

The peculiar arrangement of His161 suggested a thorough investigation on its behavior. Table 2 reports the pK_a values computed for this aminoacid in the conformations of BLG C terminus obtained with the LowModeMD approach. As reported under "Materials and methods", only the top-scoring 11 conformations were analyzed in detail. Figure 5c graphically depicts the structure of the BLG C terminus in these conformations. The backbone between Glu157 and Cys160 populates two favorite conformations, whereas the last two residues (including His161) show a marked end-effect with very high RMSD values for His161 side chain. Six of the 11 His161 conformations feature a buried side chain with a very low computed pK_a value. On the contrary, in the other five

Table 1 pK_a values for all titratable aminoacid side chains of BLG isoform A (*left*) and B (*right*) in their folded and unfolded conformations, in comparison with model values

Isoform A					Isoform B				
Residue	pK model	$pK_{a\ unfolded}$	$pK_{a\ native}$	ΔpK_a	Residue	pK model	$pK_{a\ unfolded}$	$pK_{a\ native}$	ΔpK_a
Leu1	8.0	7.93	7.65	0.28	Leu1	8.0	7.93	7.65	0.28
Lys8	10.5	10.50	10.50	0.00	Lys8	10.5	10.50	10.50	0.00
Asp11	3.8	3.82	3.65	0.17	Asp11	3.8	2.51	3.68	−1.17
Lys14	10.5	10.50	10.43	0.07	Lys14	10.5	10.36	10.36	0.00
Tyr20	10	10.00	12.92	−2.92	Tyr20	10.0	10.00	13.15	−3.15
Asp28	3.8	3.09	2.46	0.63	Asp28	3.8	3.72	2.42	1.30
Asp33	3.8	3.14	4.22	−1.08	Asp33	3.8	4.02	4.22	−0.20
Arg40	12.5	12.5	13.51	−1.01	Arg40	12.5	12.29	13.52	−1.23
Tyr42	10	10.00	7.79	2.21	Tyr42	10.0	12.61	8.01	4.60
Glu44	***4.5***	***4.50***	***5.50***	***−1.00***	*Glu44*	*4.5*	*4.50*	*5.09*	*−0.59*
Glu45	4.5	4.50	4.71	−0.21	Glu45	4.5	4.50	4.71	−0.21
Lys47	10.5	10.50	10.22	0.28	Lys47	10.5	10.5	10.36	0.14
Glu51	4.5	4.13	3.97	0.16	Glu51	4.5	4.57	3.33	1.24
Asp53	3.8	2.80	3.43	−0.63	Asp53	3.8	3.78	3.40	0.38
Glu55	4.5	4.05	4.01	0.04	Glu55	4.5	4.50	4.54	−0.04
Lys60	10.5	10.36	9.59	0.77	Lys60	10.5	10.15	10.15	0.00
Glu62	4.5	4.13	4.14	−0.01	Glu62	4.5	4.50	4.50	0.00
Asp64	3.8	3.87	4.01	−0.14					
Glu65	4.5	4.12	4.50	−0.38	Glu65	4.5	4.57	3.87	0.70
Lys69	10.5	10.50	10.36	0.14	Lys69	10.5	10.01	10.43	−0.42
Lys70	10.5	10.22	10.08	0.14	Lys70	10.5	10.43	10.36	0.07
Glu74	4.5	4.42	4.34	0.08	Glu74	4.5	4.57	4.50	0.07
Lys75	10.5	10.43	10.50	−0.07	Lys75	10.5	10.29	10.36	−0.07
Lys77	10.5	10.43	10.50	−0.07	Lys77	10.5	10.5	10.50	0.00
Lys83	10.5	10.01	10.50	−0.49	Lys83	10.5	10.29	10.50	−0.21
Asp85	3.8	3.21	3.80	−0.59	Asp85	3.8	3.85	3.80	0.05
Glu89	***4.5***	***4.50***	***6.26***	***−1.76***	***Glu89***	***4.5***	***4.28***	***6.69***	***−2.41***
Lys91	10.5	10.50	10.50	0.00	Lys91	10.5	10.50	10.43	0.07
Asp96	3.8	3.80	2.69	1.11	Asp96	3.8	2.19	2.72	−0.53
Asp98	3.8	4.01	1.67	2.34	Asp98	3.8	2.93	1.77	1.16
Tyr 99	10	10.06	10.07	−0.01	Tyr99	10	10.00	10.11	−0.11
Lys100	10.5	10.43	10.01	0.42	Lys100	10.5	10.50	10.5	0.00
Lys101	10.5	10.5	10.29	0.21	Lys101	10.5	10.15	10.36	−0.21
Tyr102	10	9.43	14.99	−5.56	Tyr102	10	10.00	14.8	−4.8
Glu108	4.5	4.11	3.05	1.06	Glu108	4.5	4.50	3.73	0.77
Glu112	4.5	4.57	4.25	0.32	Glu112	4.5	4.50	4.64	−0.14
Glu114	4.5	4.63	4.85	−0.22	Glu114	4.5	4.50	4.50	0.00
Cys121	9	7.28	10.56	−3.28	Cys121	9.0	9.00	10.54	−1.54
Arg124	12.5	11.52	11.10	0.42	Arg124	12.5	12.29	10.96	1.33
Glu127	4.5	4.64	3.98	0.66	Glu127	4.5	3.37	4.21	−0.84
Asp129	3.8	3.70	2.91	0.79	Asp129	3.8	4.15	3.13	1.02
Asp130	3.8	3.71	3.8	−0.09	Asp130	3.8	3.61	3.79	−0.18
Glu131	4.5	3.91	4.43	−0.52	Glu131	4.5	4.5	4.50	0.00
Glu134	4.5	3.92	4.50	−0.58	Glu134	4.5	4.57	3.77	0.80
Lys135	10.5	10.29	10.43	−0.14	Lys135	10.5	10.29	10.5	−0.21
Asp137	3.8	4.08	3.31	0.77	Asp137	3.8	3.21	3.63	−0.42

Table 1 continued

Isoform A					Isoform B				
Residue	*pK* model	$pK_{a\ unfolded}$	$pK_{a\ native}$	ΔpK_a	Residue	*pK* model	$pK_{a\ unfolded}$	$pK_{a\ native}$	ΔpK_a
Lys138	10.5	10.43	10.43	0.00	Lys138	10.5	10.15	10.29	−0.14
Lys141	10.5	10.50	10.50	0.00	Lys141	10.5	10.36	10.22	0.14
His146	6.5	7.63	7.44	0.19	His146	6.5	7.00	6.61	0.39
Arg148	12.5	12.22	11.90	0.32	Arg148	12.5	12.50	12.01	0.49
Glu157	4.5	4.22	3.98	0.24	Glu157	4.5	4.20	4.05	0.15
Glu158	4.5	4.64	4.71	−0.07	Glu158	4.5	3.67	4.64	−0.97
His161	***6.5***	***6.50***	***3.73***	***2.77***	***His161***	***6.5***	***6.50***	***3.69***	***2.81***
Ile162	3.2	3.32	3.41	−0.09	Ile162	3.2	3.62	3.48	0.14

Italics highlights aminoacids satisfying condition (1) reported in "Materials and methods"; bold highlights aminoacids satisfying condition (2) reported in "Materials and methods"

pK model, intrinsic pK_a of the group—the component which is independent of environment; pK_a predicted, pK_a value of the group according to the MOE Residue *pK*a program (please see "Materials and methods"); ΔpK_a, difference between pK_a unfolded–pK_a native

conformations, His161 is not buried, with pK_a values >6 and very similar to the model value.

Supplementary Table 2 reports the computed pK_a values of His161 for all the available BLG structures retrieved from the RCSB database. We retrieved 21 entries; we did not consider four of them since the position of His161 atoms was not defined. Of the others, two were obtained by NMR, and 15 were solved by X-ray diffraction. All the BLG structure solved by X-ray diffraction show the His161 side chain in a buried conformation, and with a very low pK_a value ($2.50 < pK_a < 4.26$). On the contrary, all the BLG structures contained in the two NMR files (10 and 21 conformations, respectively) show a non-buried His161 side chain, associated with pK_a values from 6.36 to 8.10.

The difference between the TCs of folded and unfolded BLG may be seen, with some blurring, in the migration pattern of the protein sample dissolved in urea and run in a gel without urea (0 M panel of Fig. 4b). Refolding does not go to completion, and two tracings of similar intensity, crossing the 0 mobility trench at different p*I*, and even staining with different color shades (Supplementary Figure 2), may be observed, somewhat in accordance with the reported changes in surface hydrophobicity of various BLG conformers (Barbiroli et al. 2010; Fessas et al. 2001; Iametti et al. 1996, 1998; Lozinsky et al. 2006; Rasmussen et al. 2007). The more alkaline species has same p*I* and the same overall ETC as native BLG (sample dissolved in buffer, in the same panel); a higher p*I* for native (or refolded) than for unfolded BLG agrees with the evidence in Fig. 4a.

At intermediate urea concentrations, the shape of the ETC for the protein dissolved in buffer progressively approaches the course typical of the unfolded protein. At alkaline pH, this coincidence is attained already in the 2 M urea medium, whereas around neutral pH it requires >4 M urea. The proportion of the protein dissolved in 8 M urea that refolds to give an ETC parallel to the protein loaded under native conditions progressively decreases; in 4 M urea, only the acidic portion is still visible.

Table 2 *pK*a values and solvent accessibility for His161 side chain of eleven C terminus 3BLG conformations obtained by LowModeMD

BLG	His161 native pK_a	Solvent accessibility
Conformation 1	2.78	Buried
Conformation 2	6.36	Non-buried
Conformation 3	2.86	Buried
Conformation 4	2.86	Buried
Conformation 5	2.87	Buried
Conformation 6	2.88	Buried
Conformation 7	6.43	Non-buried
Conformation 8	4.06	Buried
Conformation 9	6.43	Non-buried
Conformation 10	6.47	Non-buried
Conformation 11	6.88	Non-buried

Taken together, these findings indicate that the native BLG structure is more stable at acidic than at alkaline pH, in agreement with our previous results with DGGE at varying pH (Beringhelli et al. 2002) and with other literature data (D'Alfonso et al. 2002; Fogolari et al. 2000; Rochu et al. 1999; Shalabi and Fox 1982).

Discussion

The overall set of electrophoretic data obtained for BLG isoforms either in the absence or in the presence of a chaotrope demonstrates a decrease in p*I* between the folded and the unfolded protein, which is connected with a change

in the protein ETC. It is a long established assumption that in an unfolded protein: (1) all the aminoacid side chains are fully solvated; (2) no interaction occurs among them; (3) the dissociable groups display their typical model pK_a values. Under this assumption, we may take the TC of BLG in 8 M urea as representative of the overall aminoacid composition. Indeed, the experimental ETC in 8 M urea closely matches the computed TC (when the former is corrected for the slight non-linearity of the pH gradient across the gel; see Supplementary Figure 3).

Comparing to the theoretical TC the ETC under native conditions, we must conclude that in the folded protein some residues display an anomalous pK_a. The displacement of the native versus the 8 M urea ETC and the details of both native and 2 M urea ETC suggest that more than one residue is involved, and that the affected residues have dissimilar pK_a values in native BLG. In fact, the shape of the curve changes progressively with increasing urea concentration and different pH regions are affected. This suggests a range of effects from minor variations associated with microenvironment that are already lost at a low urea concentration to major interactions that require high urea concentration to be broken. The electrophoretic data cannot go any further suggesting which specific aminoacids are implied, whereas computational tools may provide atomic resolution and detailed individual characterization.

Electrostatics in BLG has already been explored in the past. In 1959, Tanford et al. (1959) observed a peculiar behavior during BLG titration: a carboxylic side chain showed a pK_a value of 7.3 and appeared to be solvent exposed in a basic environment, whereas it was buried when in an acidic environment; the underlying pH-dependent structural rearrangement was hence dubbed the Tanford transition. Hints to identify the aminoacid with anomalous behavior were provided by the BLG crystallographic structures obtained at different pH values by Qin et al. (Qin et al. 1998). Fogolari et al. (2000) then compared the pK_a computed for different BLG models with the experimental values obtained by NMR measurements. Glu89 showed an unusually high pK_a, which ranged from 4.1 to 6.8, depending on the BLG model. Later on, our research group studied in detail the role of Glu89 in the Tanford transition, finding a peculiar value for the pK^{half} of this residue, identical to the one measured by Tanford in 1959 (Eberini et al. 2004). We could connect the stabilization of Glu89 protonation state with extremely persistent H-bond interactions: the carboxylic groups are bound for 92% of the simulated time with the backbone of Ser116 (Ser116O) and for an additional 5% of the time with an alternative acceptor.

Fogolari et al. (2000) carried out an exhaustive computation, calculating the pK_a values for all the BLG titratable residues; some of their data can be directly compared with those reported in the present paper. Specifically, we are interested in residues with pK_a values that in the native and unfolded states encompass the theoretical p*I* value of both the BLG isoforms (see "Materials and methods") as they only have influence on its value. Making reference to these aminoacids, there is a partial agreement between our results (in Table 1) and those of Fogolari et al., both computed and experimental. In detail, our and their pK_a values are in very good agreement for Glu44, Glu89, and Glu114, but differ significantly for His161. For this residue, the spread among the pK_a computed by Fogolari et al. with reference to various protein models is as high as 5 *pK* units.

Fig. 5 Interactions (**a**) and lack of solvent exposure (**b**) for His161 in native BLG. In *panel a*, residues within 4.5 Å of His161 is shown (*stick* representation); hydrogen bonds are marked as *dotted lines*. In *panel b*, the molecular surface of His161 is rendered as a *solid* (*gold*), while the exposed area of the residues near His161 is mapped with *mesh surface* representation (*red*). The overall shape of the protein may be seen as *ribbon* representation; the foremost aminoacids are not rendered for clarity. (**c**) Superposition of the 3BLG C terminus conformations obtained by LowModeMD; protein backbone is rendered in *ribbons*, whereas His161 side chains are rendered as *sticks* ▶

From a molecular point of view, the His161 side chain in both isoform A and isoform B appears to be completely buried, as depicted in Fig. 5a and b, drawn from the 3BLG crystallographic structure. This evidence is confirmed by the conspicuous contributions of global and local desolvation effects to the pK_a value in BLG native form, which amount, respectively, to −1.05 and −2.73 pK units. According to our calculations, global and local desolvation is the main determinant as for the pK_a values of Glu44, Glu89, and Glu114 (Supplementary Table 1). Conversely, for His161, the formation of hydrogen bond(s) could add up to the already large desolvation contributions to determine the computed pK_a value.

However, since His161 is an aminoacid of the BLG C terminus, the end-effect associated to a solvated form of the protein can seriously influence the spatial arrangement, the interaction network, and thus the pK_a value. For evaluating this possibility, the flexibility of the 3BLG C terminus was investigated at an atomic level through a LowModeMD approach, which has already been successfully used for studying the P-loop conformations of Rho-kinase (Gohda and Hakoshima 2008) and the c-jun N-terminal kinase JNK3 (Kolossváry and Keserü 2001). This approach allowed us to sample some 3BLG C terminus conformations with a non-buried His161, associated with pK_a similar to the model value (Table 2), which suggests that His161 pK_a value seems to be very sensitive to the local conformation.

Since the very low pK_a value for His161 could be peculiar to 3BLG, we analyzed the same residue in all the BLG structures retrieved from the RCSB database. All the

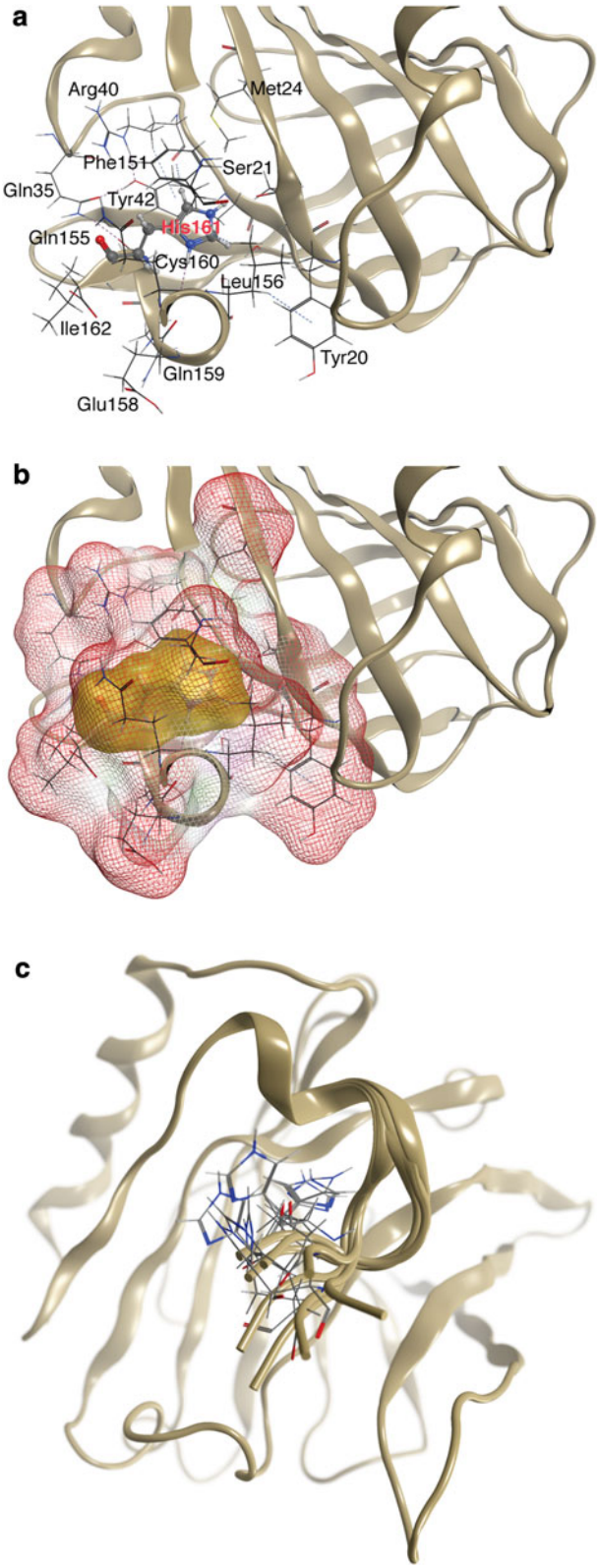

crystallographic structures showed a buried His161 associated with a very low pK_a value. On the contrary, all the NMR structures (for a total of 31 conformations) showed a non-buried His161, with pK_a closer to the model value. On contrary to the solid crystallographic structures, the NMR conformations are obtained in solution, and in more relaxed conditions. The LowModeMD allowed us to specifically relax the C terminus of BLG, removing the bias introduced by crystallization, and to obtain conformations more similar to the NMR structures. These two lines of evidence point to a dynamic end-effect associated with high mobility in BLG C terminus, which entails high fluctuations for native pK_a values. Accordingly, His161 is not expected to be especially relevant in determining the difference observed between the native and unfolded pI values for BLG in solution.

This investigation confirms that electrophoretic techniques are very effective in monitoring the heterogeneity of a protein sample and allows finely monitoring its changes. Specifically, the non-conventional procedures used here clearly display the relationship between pH and unfolding progression. As expected, the in silico procedures are able to associate specific features to individual aminoacid residues, but require a defined structural model to be applied to, and as such are easily implemented only on native or fully unfolded conformations.

Conflict of interest None.

References

Aguilar B, Anandakrishnan R, Ruscio JZ, Onufriev AV (2010) Statistics and physical origins of pK and ionization state changes upon protein-ligand binding. Biophys J 98:872–880

Barbiroli A, Beringhelli T, Bonomi F, Donghi D, Ferranti P, Galliano M, Iametti S, Maggioni D, Rasmussen P, Scanu S, Vilardo MC (2010) Bovine beta-lactoglobulin acts as an acid-resistant drug carrier by exploiting its diverse binding regions. Biol Chem 391:21–32

Beringhelli T, Eberini I, Galliano M, Pedoto A, Perduca M, Sportiello A, Fontana E, Monaco HL, Gianazza E (2002) pH and ionic strength dependence of protein (un)folding and ligand binding to bovine β-lactoglobulins A and B. Biochemistry 41:15415–15422

Bjellqvist B, Ek K, Righetti PG, Gianazza E, Görg A, Postel W, Westermeier R (1982) Isoelectric focusing in immobilized pH gradients: principles, methodology and some applications. J Biochem Biophys Methods 6:317–339

Creighton TE (1979) Electrophoretic analysis of the unfolding of proteins by urea. J Mol Biol 129:235–264

Creighton TE (1980) Kinetic study of protein unfolding and refolding using urea gradient electrophoresis. J Mol Biol 137:61–80

D'Alfonso L, Collini M, Baldini G (2002) Does β-lactoglobulin denaturation occur via an intermediate state? Biochemistry 41:326–333

Eberini I, Baptista AM, Gianazza E, Fraternali F, Beringhelli T (2004) Reorganization in apo- and holo-β-lactoglobulin upon protonation of Glu89: molecular dynamics and pKa calculations. Proteins 54:744–758

Ellis RJ, van der Vies SM (1991) Molecular chaperones. Annu Rev Biochem 60:321–347

Fessas D, Iametti S, Schiraldi A, Bonomi F (2001) Thermal unfolding of monomeric and dimeric beta-lactoglobulins. Eur J Biochem 268:5439–5448

Fogolari F, Ragona L, Licciardi S, Romagnoli S, Michelutti R, Ugolini F, Molinari H (2000) Electrostatic properties of bovine β-lactoglobulin. Proteins 39:317–330

Gianazza E, Giacon P, Sahlin B, Righetti PG (1985) Non-linear pH courses with immobilized pH gradients. Electrophoresis 6:53–56

Gianazza E, Galliano M, Miller I (1997) Structural transitions of human serum albumin: an investigation using electrophoretic techniques. Electrophoresis 18:695–700

Gianazza E, Castiglioni S, Eberini I (1999) Low-tech electrophoresis, small but beautiful, and effective: electrophoretic titration curves of proteins. Electrophoresis 20:1325–1338

Gitlin I, Carbeck JD, Whitesides GM (2006) Why are proteins charged? Networks of charge-charge interactions in proteins measured by charge ladders and capillary electrophoresis. Angew Chem Int Ed Engl 45:3022–3060

Gohda K, Hakoshima T (2008) A molecular mechanism of P-loop pliability of Rho-kinase investigated by molecular dynamic simulation. J Comput Aided Mol Des 22:789–797

Goldberg AL (2003) Protein degradation and protection against misfolded or damaged proteins. Nature 426:895–899

Goldenberg DP (1989) Analysis of protein conformation by gel electrophoresis. In: Creighton TE (ed) Protein structure: a practical approach. IRL Press, Oxford, pp 225–250

Goldenberg NM, Steinberg BE (2010) Surface charge: a key determinant of protein localization and function. Cancer Res 70:1277–1280

Harris TK, Turner GJ (2002) Structural basis of perturbed pKa values of catalytic groups in enzyme active sites. IUBMB Life 53:85–98

Iametti S, De Gregori B, Vecchio G, Bonomi F (1996) Modifications occur at different structural levels during the heat denaturation of beta-lactoglobulin. Eur J Biochem 237:106–112

Iametti S, Scaglioni L, Mazzini S, Vecchio G, Bonomi F (1998) Structural features and reversible association of different quaternary structures of β-lactoglobulin. J Agric Food Chem 46:2159–2166

Iametti S, Rasmussen P, Frokiaer H, Ferranti P, Addeo F, Bonomi F (2002) Proteolysis of bovine beta-lactoglobulin during thermal treatment in subdenaturing conditions highlights some structural features of the temperature-modified protein and yields fragments with low immunoreactivity. Eur J Biochem 269:1362–1372

Juffer AH (1998) Theoretical calculations of acid-dissociation constants of proteins. Biochem Cell Biol 76:198–209

Kolossváry I, Keserü GM (2001) Hessian-free low-mode conformational search for large-scale protein loop optimization: application to c-jun N-terminal kinase JNK3. J Comput Chem 22:21

Labute P (2010) LowModeMD—implicit low-mode velocity filtering applied to conformational search of macrocycles and protein loops. J Chem Inf Model 50:792–800

Lanni C, Uberti D, Racchi M, Govoni S, Memo M (2007) Unfolded p53: a potential biomarker for Alzheimer's disease. J Alzheimers Dis 12:93–99

Lee AC, Crippen GM (2009) Predicting pKa. J Chem Inf Model 49:2013–2033

Li H, Robertson AD, Jensen JH, Vacca JP (2005) Very fast empirical prediction and rationalization of protein pKa values. Proteins 61:704–721

Lozinsky E, Iametti S, Barbiroli A, Likhtenshtein GI, Kalai T, Hideg K, Bonomi F (2006) Structural features of transiently modified beta-lactoglobulin relevant to the stable binding of large hydrophobic molecules. Protein J 25:1–15

Monaco HL, Zanotti G, Spadon P, Bolognesi M, Sawyer L, Eliopoulos EE (1987) Crystal structure of the trigonal form of bovine β-lactoglobulin and of its complex with retinol at 2.5 Å resolution. J Mol Biol 197:695–706

Mulgrew-Nesbitt A, Diraviyam K, Wang J, Singh S, Murray P, Li Z, Rogers L, Mirkovic N, Murray D (2006) The role of electrostatics in protein-membrane interactions. Biochim Biophys Acta 1761:812–826

Nakamura H (1996) Roles of electrostatic interaction in proteins. Q Rev Biophys 29:1–90

Neves-Petersen MT, Petersen SB (2003) Protein electrostatics: a review of the equations and methods used to model electrostatic equations in biomolecules—applications in biotechnology. Biotechnol Annu Rev 9:315–395

Nielsen JE, McCammon JA (2003) Calculating pKa values in enzyme active sites. Protein Sci 12:1894–1901

Pace CN, Grimsley GR, Scholtz JM (2009) Protein ionizable groups: pK values and their contribution to protein stability and solubility. J Biol Chem 284:13285–13289

Qin BY, Bewley MC, Creamer LK, Baker HM, Baker EN, Jameson GB (1998) Structural basis of the Tanford transition of bovine β-lactoglobulin. Biochemistry 37:14014–14023

Rasmussen P, Barbiroli A, Bonomi F, Faoro F, Ferranti P, Iriti M, Picariello G, Iametti S (2007) Formation of structured polymers upon controlled denaturation of beta-lactoglobulin with different chaotropes. Biopolymers 86:57–72

Righetti PG (1990) Immobilized pH gradients: theory and methodology. Elsevier, Amsterdam

Righetti PG, Drysdale JW (1974) Isoelectric focusing in gels. J Chromatogr 98:271–321

Righetti PG, Gianazza E (1980) pH-mobility curves of proteins by isoelectric focusing combined with electrophoresis at right angle. In: Radola BJ (ed) Electrophoresis '79. W. de Gruyter, Berlin, pp 23–38

Rochu D, Ducret G, Ribes F, Vanin S, Masson P (1999) Capillary zone electrophoresis with optimized temperature control for studying thermal denaturation of proteins at various pH. Electrophoresis 20:1586–1594

Rosengren Å, Bjellqvist B, Gasparic V (1977) A simple method of choosing optimum pH conditions for electrophoresis. In: Radola BJ, Graesslin D (eds) Electrofocusing and isotachophoresis. W. de Gruyter, Berlin, pp 165–171

Schreiber G, Shaul Y, Gottschalk KE (2006) Electrostatic design of protein–protein association rates. Methods Mol Biol 340:235–249

Shalabi SI, Fox PF (1982) Heat stability of milk: influence of cationic detergents on pH sensitivity. J Dairy Res 49:597–605

Sillero A, Maldonado A (2006) Isoelectric point determination of proteins and other macromolecules: oscillating method. Comput Biol Med 36:157–166

Tanford C (1962) The interpretation of hydrogen titration curves of proteins. Adv Prot Chem 17:69–165

Tanford C, Bunville LG, Nozaki Y (1959) The reversible transformation of β-lactoglobulin at pH 7.5. J Am Chem Soc 81:4032–4036

Tyedmers J, Mogk A, Bukau B (2010) Cellular strategies for controlling protein aggregation. Nat Rev Mol Cell Biol 11:777–788

Vizcarra CL, Mayo SL (2005) Electrostatics in computational protein design. Curr Opin Chem Biol 9:622–626

Wilson MR, Yerbury JJ, Poon S (2008) Potential roles of abundant extracellular chaperones in the control of amyloid formation and toxicity. Mol Biosyst 4:42–52